



Synthesis and structure of iron (III) and iron (II) complexes in S_4P_2 environment created by diethyldithiocarbamate and 1,2-bis(diphenylphosphino)ethane chelation: Investigation of the electronic structure of the complexes by Mössbauer and magnetic studies

Tanmay K. Jana^a, Dhurjati P. Kumar^a, Rabindranath Pradhan^{a,c}, Subhajit Dinda^a, Pradip N. Ghosh^a, Corine Simonnet^b, Jérôme Marrot^b, Inhar Imaz^c, Alain Wattiaux^c, Léopold Fournès^c, Jean-Pascal Sutter^{c,d,*}, Francis Sécheresse^{b,*}, Ramgopal Bhattacharyya^{a,*}

^a Department of Chemistry, Jadavpur University, Kolkata, West Bengal 700032, India

^b Institut Lavoisier, Université de Versailles Saint-Quentin-en-Yvelines, 45, Avenue des Etats Unis, F-78035 Versailles Cedex, France

^c Institut de Chimie de la Matière Condensée de Bordeaux-CNRS, Université Bordeaux 1, F-33608 Pessac, France

^d Laboratoire de Chimie de Coordination du CNRS, Université Paul Sabatier, F-31077 Toulouse, France

ARTICLE INFO

Article history:

Received 11 October 2008

Received in revised form 19 March 2009

Accepted 3 April 2009

Available online 18 April 2009

Keywords:

Iron complexes

Sulfur and phosphorous donors

Crystal structure

Mössbauer spectra

Magnetic studies

Cyclic voltammetry

ABSTRACT

Iron (II) and iron (III) complexes, $[\text{Fe}^{\text{II}}(\text{DEDTC})_2(\text{dppe})] \cdot \text{CH}_2\text{Cl}_2$ (**1**), $[\text{Fe}^{\text{II}}(\text{ETXANT})_2(\text{dppe})]$ (**2**) (DEDTC = diethyldithiocarbamate, ETXANT = ethyl xanthate, dppe = 1,2-bis(diphenylphosphino)ethane), and $[\text{Fe}^{\text{III}}(\text{DEDTC})_2(\text{dppe})][\text{Fe}^{\text{III}}\text{Cl}_4]$ (**3**) have been synthesized and characterized. Since **3** contains two magnetic centers, an anion metathesis reaction has been conducted to replace the tetrahedral FeCl_4^- by a non-magnetic BPh_4^- ion producing $[\text{Fe}^{\text{III}}(\text{DEDTC})_2(\text{dppe})]\text{BPh}_4$ (**4**) for the sake of unequivocal understanding of the magnetic behavior of the cation of **3**. With the similar end in view, the well-known FeCl_4^- ion, the counter anion of **3**, is trapped as $\text{PPh}_4[\text{Fe}^{\text{III}}\text{Cl}_4]$ (**5**) and its magnetic property from 298 to 2 K has been studied. Besides the spectroscopic (IR, UV-Vis, NMR, EPR, Mass and XPS) characterization of the appropriate compounds, especially **2**, others viz. **1**, **3** and **4** have been structurally characterized by X-ray crystallography. While Fe^{II} complexes, **1** and **2**, are diamagnetic, the Fe^{III} systems, namely the cations of **3**, and **4** behave as low-spin ($S = 1/2$) paramagnetic species from 298 to 50 K. Below 50 K **3** shows gradual increase of $\chi_M T$ up to 2 K suggesting ferromagnetic behavior while **4** exhibits gradual decrease of magnetic moment from 60 to 2 K, indicating the occurrence of weak antiferromagnetic interaction. These conclusions are supported by the Mössbauer studies of **3** and **4**. The Mössbauer pattern of **1** exhibits a doublet site for diamagnetic (2–400 K) Fe^{II} . The compounds **1**, **2** and **4** encompass interesting cyclic voltammetric responses involving Fe^{II} , Fe^{III} and Fe^{IV} .

© 2009 Published by Elsevier B.V.

1. Introduction

Pioneering observation of Cambi and Szego [1,2] of the unusual temperature dependence of magnetic moments of various tris-(*N,N*-dialkyldithiocarbamate) iron (III) complexes was attributed [3] to the spin-crossover phenomenon in octahedral transition metal complexes originating from two types of arrangements of the five 3d electrons depending on the strength of the ligand field. Recent discovery of the application of spin-transition systems in optoelectronics [4,5], information storage [6,7], imparting special

properties to liquid crystalline materials [8] and to the naturally occurring spin crossover type Fe(III)-porphyrin systems [9,10] stimulated an enormous interest in the synthesis and study of new spin-transition complexes. It is well known that strength of crystal field splitting parameter, Δ_o (of octahedral transition metal complexes) can be expressed as $\Delta_o = f \times g$, where f = the field strength of the ligands and the g -factor is the characteristic of the actual metal ions involved [11]. The field strength of the ligands depends largely on the donor atoms, which can be arranged in increasing ligand field order as CISONPC; the metal g -factor, with its usual trends also depends on the oxidation states of metal ions concerned. In this regard the cases of Co^{II} and Fe^{II} in octahedral environment are interesting. Co^{II} when bound to strong field ligands generates Co^{III} complexes and the reverse is the case for Fe^{II} , which is very much stable when surrounded by strong field ligands, but becomes oxidized to Fe^{III} when liganded with weak field

* Corresponding authors. Tel.: +91 33 24327159; fax: +91 33 24137902.

E-mail addresses: sutter@lcc-toulouse.fr (J.-P. Sutter), secheresse@uvsq.chimie.fr (F. Sécheresse), aargibhatta@yahoo.com (R. Bhattacharyya).

¹ Tel.: +33 561333157; fax: +33 561553003.

² Tel.: +33 139254389; fax: +33 139254381.

species [12–16]. This is quite understandable from the pairing energy of the electrons and electronic arrangement of the above mentioned transition metal ions in their t_{2g} and e_g orbitals. The above explanation is supported by relevant E^0 and ΔG^0 values of the appropriate $\text{Co}^{\text{II}} \rightleftharpoons \text{Co}^{\text{III}}$ and $\text{Fe}^{\text{II}} \rightleftharpoons \text{Fe}^{\text{III}}$ systems. Hence, besides Fe^{III} , Co^{II} also should show spin–transition behavior and it really does so [17,18]. Fe^{III} and even Fe^{II} solutions in presence of air have a strong tendency to generate $[\text{Fe}^{\text{III}}\text{S}_6]$ functions when bidentate S–S ligands like dialkyldithiocarbamates or alkyl xanthates [19] are used, apparently indicating the weak field character of S–ligands, but since Co^{II} also displays similar behavior affording $\text{Co}(\text{S–S})_3$ where S–S = RRDTTC and RXANT, the said apparent conclusion is not tenable. Moreover, the ligand field splitting (Δ) and Racah parameter B generated by $\text{RR}'\text{NCS}_2^-$ (= $\text{RR}'\text{DTC}$ = dialkyldithiocarbamate ion) ligands in $[\text{Fe}^{\text{III}}(\text{RR}'\text{NCS}_2)_3]$ type complexes are well known [1–3] to create a situation which place the said complex at the ${}^6\text{A}_1 \rightarrow {}^2\text{T}_2$ electronic crossover [20] and changes in R substituents are known to change the position of the spin state equilibrium via the difference in their resonance, inductive and steric effect [21] apparently indicating that S–ligands of these dithio-acid groups are not typical weak field ligands like disubstituted dithiophosphates, sulfides, and thioethers and N,N' -pyrrolydyl dithiocarbamates [22]. Actually, Tanabe–Sugano diagrams which consider B as a fundamental parameter are more realistic, and considering higher covalency effect of S–ligands, (specially in Fe–S systems [23]) such as dithiocarbamates and xanthates, consideration of merely the position of these ligands in spectrochemical series should not be the only guide for expecting the electronic crossover. The mixed ligand Fe–S complexes, where, besides S–ligands other donor atoms present should be considered and given due importance. In the present paper, however, we are not reporting any new ST material, but are giving an account of a systematic study in order to arrive at a situation whereby one can have an insight in predicting the directed synthesis of spin–transition compounds. With this end in view we undertook a study on the substitution of one of the DEDTC ligand in $[\text{Fe}^{\text{III}}(\text{DEDTC})_3]$ (DEDTC = diethyldithiocarbamate) with bidentate π -acidic P-donor ligand, namely, 1,2 bis(diphenylphosphino) ethane, (dppe), which possesses high covalency as well as ligand field effect [24] to enforce a drastic change in magnetic and other behavior of the resulting compound. We expected the introduction of dppe would impose such a field strength that the ground state term of the resulting complexes would be placed at the right hand side of the respective Tanabe Sugano diagram and so the synthesized Fe (III) complexes would be the pure low-spin species without exhibiting any ST property. So it was of interest to study (i) physicochemical characterization and structure of the synthesized new mixed ligand complexes and (ii) ground state configuration and associated magnetic behavior of the compounds in the temperature range of 2–300 K to bring out magneto structural relationship in the context of the introduction of phosphorus donors in iron–sulfur environment. Hence, in this paper we report the synthesis and structure of a series of $[\text{FeS}_4\text{P}_2]$ complexes $[\text{Fe}^{\text{II}}(\text{DEDTC})_2(\text{dppe})]$ (**1**), $[\text{Fe}^{\text{II}}(\text{ETXANT})_2(\text{dppe})]$ (**2**), $[\text{Fe}^{\text{III}}(\text{DEDTC})_2(\text{dppe})][\text{Fe}^{\text{III}}\text{Cl}_4]$ (**3**) and $[\text{Fe}^{\text{III}}(\text{DEDTC})_2(\text{dppe})][\text{BPh}_4]$ (**4**). Compound **2** is not structurally characterized by X-ray crystallography but its adequate spectroscopic characterization indicate that its structure is similar to that of **1**. For the unequivocal understanding of the magnetic and Mössbauer behavior of the low-spin Fe (III) complexes **3** and **4**, we also had to prepare and characterize $\text{PPh}_4[\text{FeCl}_4]$ (**5**) [25] for the anion of which the detailed magnetic behavior below 80 K has not yet been reported but we need to know the same since it exists as counter anion in **3**, to confirm whether or not there exists any magnetic interaction between the two Fe^{III} centers at 298–50 K. Furthermore, the Fe^{III} ion being a hard acceptor, Fe^{III} –phosphorus bonds existing in **3** and **4** are formed by hard–soft interactions and so the thermodynamic and

kinetic instability of the said bonds should be the root of the interest developed along with the problem created in unequivocally interpreting the magnetic and Mössbauer behavior of those two complexes. Notably not many 3d metal complexes are known with S_4P_2 coordination sphere [26] and low-spin Fe (III) complexes are not numerous [27] compared to its high spin analogues and before 10 years their numbers were really low [12–16,27]. The recent surge of synthesis of low-spin Fe^{III} complexes and detailed studies of their electronic structure including ST behavior is mainly due to Weighardt and his group [28,29]. The aims and objective of this work is to set the right hand boundary of the mixed ligand Fe^{III} –DEDTC systems which remains a low-spin species from 2 to 300 K, with an ulterior motive to derivatize the ligands used or to change the ring size of the P–P chelates so that the resulting Fe (III) complexes may show spin–transition properties. Similarly, the left hand boundary (the resulting Fe (III) complexes showing pure high spin behavior from 2 to 300 K) can be set in our forthcoming work by replacing P–P chelates by N–N chelates. Both the boundaries being thus known, we hope to play in the mid-field to take command over the situation, leading to the discoveries of diverse spin–crossover systems.

2. Experimental

2.1. Materials

Anhydrous iron (III) chloride, iron (II) chloride, 1,2-bis(diphenylphosphino)ethane (dppe) were obtained from Aldrich and used as received. Iron (II) chloride tetrahydrate, Mohr's salt $[\text{FeSO}_4 \cdot (\text{NH}_4)_2\text{SO}_4 \cdot 6\text{H}_2\text{O}]$, tetraethylammonium chloride and tetraphenylphosphonium chloride of G.R. grade were obtained from E. Merck (Germany). Acetonitrile, nitrobenzene, dichloromethane, hexane, carbon disulfide, P_4O_{10} , KOH and NaClO_4 of G.R. grade were obtained from E. Merck (India). Sodium salt of diethyl dithiocarbamate was the extrapure product of Loba chemie (India). Ethanol (90%) was obtained from Bengal Chemicals and Pharmaceuticals Ltd., Calcutta, was treated with lime (CaO) and kept for 48 h and distilled before use. Mineral acids and alkalis were of G.R. (E. Merck, India) grade. Commercially available distilled water was further [once using KMnO_4 (G.R.)] distilled (all glass) twice and this water was used for all experimental purposes. Acetonitrile used for synthetic, spectroscopic and other physicochemical measurements was further purified by refluxing with P_4O_{10} and distilling out the solvent, which was again treated with fresh P_4O_{10} , refluxed and distilled and the process was repeated until a fresh P_4O_{10} was not stained yellow when added to the last (fresh) distillate. For electrochemical studies this solvent was further purified by treatment with CaH_2 (overnight) followed by successive distillation over Li_2CO_3 , KMnO_4 and P_4O_{10} . Pure tetraethyl ammonium perchlorate (for electrochemical studies) was obtained by the anion metathesis of tetraethyl ammonium chloride with perchloric acid in aqueous medium and then recrystallizing the product from water. The quality of other chemicals used is mentioned in proper places in the text. Potassium *o*-ethyl xanthate was synthesized from carbon disulfide, ethanol and KOH, following literature procedure [30].

2.2. Physical measurements

Electrolytic conductance in CH_3CN solution was measured on a Philips PR 9500 conductivity bridge and the molecular weights of the complexes were determined in nitromethane solution using a KNAUR (Berlin) vapor pressure osmometer using benzyl (PhCOCOPh) as a calibrant. Infrared spectra in the range 4000–200 cm^{-1} were recorded using a Perkin–Elmer 597 IR spectrophoto-

tometer and those in the range 4000–400 cm^{-1} , using a Perkin–Elmer 883 FT-IR spectrophotometer. The electronic spectra were obtained on a Hitachi model U-3410 UV–Vis–NIR spectrophotometer and when required, by Perkin–Elmer Lambda 25 UV–Vis–NIR spectrophotometer attached with GAUSSIAN03 W attachment. The ^1H NMR spectrum of **1** in CDCl_3 was recorded with a Varian EM 390 spectrometer using TMS as a calibrant and the ^{13}C NMR spectrum was recorded in a BRUKER DPX-300 spectrometer using the same calibrant in CDCl_3 . The EI mass spectrum of **1** was recorded on a Varian MS 9 mass spectrometer operating at a pressure of 10^{-8} mm of Hg at 70 eV. Perfluorobutyl amine (Fischer analytical) was used as a calibrant. FAB mass spectra in a *m*-nitrobenzyl alcohol (G.R., E. Merck) matrix were obtained by using a Jeol SX 102 mass spectrometer applying the DA-6000 data system and utilizing xenon as the FAB gas. The electrospray mass spectrum of **3** was recorded on a MICROMASS QUATTRO-II triple-Quadrupole spectrometer. The magnetic measurements of **3**, **4** and **5** have been performed with a Quantum design MPMS-5S Squid magnetometer. The temperature dependence of the molar magnetic susceptibility, χ_M , for each compound was collected in the temperature range 2–300 K. The data have been corrected for diamagnetic contributions deduced from Pascal's constants. The field dependence of magnetization at 2 K was measured up to 5 T.

The Mössbauer spectra were recorded on a HALDER spectrometer with a constant acceleration and a ^{57}Co source (Rh matrix) working at room temperature. The finely ground powdered samples containing ca. 10 mg iron/ cm^2 were maintained in an airtight holder between two aluminum foils. For such concentration line broadening effects can be neglected. Isomer shifts are expressed with respect to α -Fe at 293 K. For each of the compounds **3**, **4** and **5** data have been collected at 293 K and 4.2 K. Spectra fittings have been carried out into two stages. First Lorentzian peak profile was assumed and the position, amplitude, and width of each peak were refined. This preliminary analysis allowed to determine the experimental hyperfine parameter for the various iron sites present in the compounds. When the width was too large, a second refinement was performed in terms of quadrupole splitting distribution, $P(\Delta)$, and hyperfine field distribution, $P(H)$, using the method of Hesse and Rubartsch [31]. This method is often used for materials showing disorder and a significant surrounding distribution, which give rise to strong line broadening and a line shape deviating from a Lorentzian profile. In the procedure, the band widths (Γ) are fixed (typically between 0.40 and 0.25 mm s^{-1}) and the isomer shifts (δ) used are deduced by fitting a Lorentzian profile to the experimental data. For each Fe site, either a distribution of a quadrupole splitting or a distribution of hyperfine fields can thus be obtained from which a mean quadrupole splitting (Δ) or a mean hyperfine field (H) are deduced.

The XPS studies were carried out on an ESCALAB 503 X-ray photoelectron spectrometer. The Al $K\alpha$ line (1486.6 eV) was used as the excitation source. The spectra were calibrated by using the $\text{C}_{1s,1/2}$ binding energy (at 285.0 eV) from pump oil as an internal standard [32,33]. Electrochemical measurements like cyclic voltammetry were done by using a PAR model 378-1 electrochemistry system incorporating the following components: 174 A polarographic analyzer, 175 universal programmer, RE 0074 XY recorder, 173 potentiostat and 377 cell system. All experiments were performed under a nitrogen atmosphere. A stout platinum wire working electrode, a platinum foil auxiliary electrode and an aqueous saturated calomel reference electrode (SCE) were used in the three electrode configuration. All experimental data were collected at 298 K and are uncorrected for the junction potentials. The data were also calibrated observing ferrocene–ferrocenium couple under the same experimental condition. X-ray powder diffractograms were recorded with a XRD powder diffractometer (PW 1730/1770) at 22 °C operating at 40 kV and 20 mA with 2°min^{-1} scan rate. In

the cases of special equipments necessary for a particular experiment, the details of those will be quoted in the proper place.

2.3. Preparation of the complexes

2.3.1. $[\text{Fe}^{\text{II}}\{(\text{C}_6\text{H}_5)_2\text{NS}_2\}_2]\{(\text{C}_6\text{H}_5)_2\text{P-CH}_2\text{-CH}_2\text{-P}(\text{C}_6\text{H}_5)_2\} \cdot \text{CH}_2\text{Cl}_2$: $[\text{Fe}^{\text{II}}(\text{dppe})(\text{DEDTC})_2] \cdot \text{CH}_2\text{Cl}_2$ (**1**)

Method 1 from Fe (II) starting material: $\text{FeCl}_2 \cdot 4\text{H}_2\text{O}$ (0.25 g; 1.25 mmol) was dissolved in 15 mL of ethanol and to it a CH_2Cl_2 (30 mL) solution of dppe (0.76 g; 1.9 mmol) was added under nitrogen atmosphere. An ethanolic solution (10 mL) of Na-DEDTC $\cdot 3\text{H}_2\text{O}$ (0.56 g; 2.48 mmol) was added dropwise to the above solution under stirring while a green compound separated. The product was filtered off and washed with ethanol (0.5 mL) and diethyl ether. The compound thus obtained was recrystallized from CH_2Cl_2 –hexane mixture (6:1) to obtain deep green needles. Yield 0.210 g (55%). *Anal. Calc.* for $\text{C}_{37}\text{H}_{46}\text{N}_2\text{S}_4\text{P}_2\text{Cl}_2\text{Fe}$: C, 53.17; H, 5.56; N, 3.35; S, 15.34; P, 7.41; Cl, 8.48; Fe, 6.68. *Found:* C, 52.5; H, 6.00; S, 17.0; P, 8.30; Cl, 7.98; Fe, 6.50%. *M.W.*, 828 g mol^{-1} . IR (KBr disc) cm^{-1} : 3120(w), 3000(w) 2960(w), 1505(s), 1430(s), 1380(w), 1360(w), 1270(s), 1230(m), 1200(w), 1150(m), 1100(w), 1020(w), 1000(w), 920(w), 880(w), 810(w), 790(w), 770(m), 740(m), 730(s), 700(s), 680(m), 500(s), 480(m), 460(m), 440(w), 370(w), 330(w), UV–Vis [$\lambda_{\text{max}}/\text{nm}$ ($\epsilon/\text{M}^{-1} \text{cm}^{-1}$)]: 288(8925), 440(1540), 585(330). The compound prepared by either ways is soluble in chloroform, dichloromethane, acetonitrile and acetone.

Method 2 from Fe (III) starting material: $\text{FeCl}_3 \cdot 6\text{H}_2\text{O}$ (0.15 g; 0.50 mmol) was dissolved in 20 mL of ethanol, warmed (60–70 °C) and to this solution a 10 mL ethanolic solution of ascorbic acid (0.53 g, 3.0 mmol) was added dropwise with stirring when the yellow brown color of the original solution was changed to yellowish green. To this, a CH_2Cl_2 (20 mL) solution of 1,2 bis (diphenylphosphino) ethane (dppe) (0.31 g, 0.77 mmol) was added while stirring and heating at $\sim 55^\circ\text{C}$. Heating and stirring were continued for another one and a half hour when an orange yellow solution resulted which was cooled to room temperature and the precipitate appeared during cooling was redissolved with minimum amount of CH_2Cl_2 . Na-DEDTC (0.23 g; 1.0 mmol) dissolved in 10 mL of 90% ethanol was then added dropwise to the above solution when a deep green solid separated. The solid was filtered off and washed with ethanol (0.5 mL) and diethyl ether. The compound was recrystallized from CH_2Cl_2 –hexane mixture (6:1) to obtain deep green needles of $[\text{Fe}(\text{dppe})(\text{DEDTC})_2] \cdot \text{CH}_2\text{Cl}_2$. Yield 0.210 g (54%). *Anal. Found:* C, 52.9; H, 5.70; N, 3.44; S, 14.8; P, 8.07; Cl, 8.01; Fe, 6.50%. *M.W.*, 795 g mol^{-1} (determined experimentally by vapor pressure osmometric method) *M.W.*, 835.78 g mol^{-1} .

2.3.2. $[\text{Fe}(\text{C}_2\text{H}_5\text{OCS}_2)_2\{(\text{C}_6\text{H}_5)_2\text{PCH}_2\text{CH}_2\text{P}(\text{C}_6\text{H}_5)_2\}] [\text{Fe}(\text{dppe})(\text{ETXANT})_2]$ (**2**)

An aqueous ethanolic (90% ethanol, 10% water, v/v) solution (10 mL) of ascorbic acid (1.06 g; 6 mmol) was slowly added with stirring to an ethanolic (90%) solution (20 mL) of $\text{FeCl}_3 \cdot 6\text{H}_2\text{O}$ (0.27 g; 1.0 mmol). The temperature of the solution was then raised to 70 °C when the yellow–brown color of the solution was discharged. To the hot solution was then added with stirring a 10 mL of dichloromethane solution of dppe (0.40 g; 1.0 mmol). Stirring and heating was continued for another 15 min. The orange yellow solution so produced was cooled to room temperature and an ethanolic (90%) solution (20 mL) of Na-ETXANT (0.32 g; 2.0 mmol) was added to it and a brown black precipitate appeared. The separated solid was filtered off, washed with water, ethanol and diethyl ether. The substance was purified by recrystallization from chloroform–diethyl ether mixture (4:1). Yield 0.62 g (88%). *Anal. Calc.* for $\text{C}_{32}\text{H}_{34}\text{O}_2\text{P}_2\text{S}_4\text{Fe}$: C, 55.17; H, 4.93; P, 8.89; S, 18.41; Fe, 8.02; *M.W.*, 696.67 g mol^{-1} . *Found:* C, 54.8; H, 5.10; P, 8.80; S, 18.1; Fe, 7.80%. *M.W.*, 680 g mol^{-1} . IR (KBr disc) cm^{-1} : 3080(w),

3060(w), 2990(w), 1588(w), 1578(w), 1482(w), 1465(w), 1435(s), 1418(w), 1403(w), 1385(m), 1295(w), 1015(m), 870(m), 800(w), 755(m), 742(m), 700(s), 678(m), 650(w), 620(w), 518(s), 478(w), 422(w), 342(w), 330(w). The powder X-ray diffractogram for this compound can be found in the supporting information (Fig. S1-1).

2.3.3. $[\text{Fe}^{\text{III}}\{(\text{C}_2\text{H}_5)_2\text{NCS}_2\}_2\{\text{C}_6\text{H}_5\}_2\text{PCH}_2\text{CH}_2\text{P}(\text{C}_6\text{H}_5)_2\}]\text{Fe}^{\text{III}}\text{Cl}_4$: $[\text{Fe}^{\text{III}}(\text{dppe})(\text{DEDTC})_2]\text{Fe}^{\text{III}}\text{Cl}_4$ (**3**)

$\text{FeCl}_3 \cdot 6\text{H}_2\text{O}$ (0.14 g; 0.50 mmol) was dissolved in 15 mL of ethanol, warmed a little and then 2–3 drops of concentrated HCl were added to the clear solution. To this solution was added dropwise an ethanol (90%, 10 mL) solution of $\text{NH}_2\text{OH} \cdot \text{HCl}$ (0.12 g, 17.2 mmol) under constant stirring, the color of the solution changed from deep brown to light yellow. The solution was warmed at 60–70 °C, stirred for 10 min, filtered through a Whatman 40 filter paper (in case of appearance of any turbidity). To the filtrate a CH_2Cl_2 (20 mL) solution of dppe (0.40 g, 1.0 mmol) was added with stirring when an orange yellow color developed. Stirring was continued for another 15–20 min and the solution was filtered out from any solid separated at this stage. The solution was then kept on a steam bath for 15 min to remove CH_2Cl_2 , cooled, and in case of separation of any precipitate, the same was dissolved by adding a minimum volume of CH_2Cl_2 . Then an ethanol (90%, 10 mL) solution of Na-DEDTC (0.12 g, 0.50 mmol) was added (concentration of DEDTC^- was kept low to avoid formation of $[\text{Fe}(\text{DEDTC})_3]$) to the clear solution, dropwise and under constant stirring. The separated black needles were filtered off, washed with water (to remove the precipitate of NaCl) and then with 90% ethanol and finally with diethyl ether. The solid was collected by filtration and was recrystallized from CH_2Cl_2 -ether (6:1) mixture to obtain shining black needles. Yield 0.21 g (55%). *Anal. Calc.* for $\text{C}_{36}\text{H}_{44}\text{N}_2\text{S}_4\text{P}_2\text{Cl}_4\text{Fe}_2$: C, 45.6; H, 4.69; N, 2.95; P, 4.53; S, 13.5; Cl, 14.95; Fe, 11.80; M.W., 948.50 g mol^{-1} . *Found*: C, 45.9; H, 4.7; N, 3.07; P, 6.60; S, 13.8; Cl, 14.09, Fe, 12.0%; M.W., 925 g mol^{-1} . IR (KBr pallet) cm^{-1} : 3020(w), 2460(w), 1515(s), 1490(w), 1470(w), 1440(s), 1390(w), 1360(w), 1280(s), 1210(w), 1160(m), 1100(m), 1000(w), 870(w), 850(w), 815(m), 750(m), 720(m), 695(s), 680(w), 650(w), 525(s), 515(m), 390(s), 380(s), 260(w). UV-Vis [$\lambda_{\text{max}}/\text{nm}$ ($\epsilon/\text{M}^{-1}\text{cm}^{-1}$): 270(2880), 360(3400), 492(125), 581(88), 662(113).

It may be noted here that the above synthetic protocol if applied by using NaETXANT instead of NaDEDTC, the compound $[\text{Fe}^{\text{II}}(\text{ETXANT})_2(\text{dppe})]$ (**2**) is generated, once again demonstrating that the ETXANT is a stronger and more reducing ligand than DEDTC. It is diamagnetic and its IR spectra is superimposable with that of **2**.

2.3.4. $[\text{Fe}^{\text{III}}\{(\text{C}_2\text{H}_5)_2\text{NCS}_2\}_2\{\text{C}_6\text{H}_5\}_2\text{PCH}_2\text{CH}_2\text{P}(\text{C}_6\text{H}_5)_2\}]\text{BPh}_4$: $[\text{Fe}(\text{dppe})(\text{DEDTC})_2]\text{BPh}_4$ (**4**)

Compound **3** (0.10 g; 0.10 mmol) was dissolved in 20 mL of ethanol and to it was added solid NaBPh_4 (0.04 g; 0.1 mmol). The mixture was stirred for 5 min when a brown black compound separated. The substance was filtered off, washed with water, ethanol and diethyl ether. The solid was then recrystallized from CH_2Cl_2 -hexane (6:1) solvent mixture. The black needles were collected and vacuum dried. Yield 0.90 g (85%). *Anal. Calc.* for $\text{C}_{60}\text{H}_{64}\text{BF}_4\text{N}_2\text{P}_2\text{S}_4$: C, 67.34; H, 6.04; N, 2.62; S, 11.98; P, 5.79; Fe, 5.22. *Found*: C, 67.1; H, 5.9; N, 2.8; S, 12.3; P, 5.7; Fe, 4.9%. IR (KBr pallet cm^{-1}): 3040(w), 2960(w), 1570(w), 1505(s), 1445(s), 1375(w), 1350(m), 1275(s), 1210(m), 1160(m), 1100(s), 1030(w), 1000(w), 865(w), 805(w), 800(w), 750(s), 730(s), 710(s), 700(s), 615(m), 530(s), 520(w), 515(w), 400(w), 265(w). UV-Vis [$\lambda_{\text{max}}/\text{nm}$ ($\epsilon/\text{M}^{-1}\text{cm}^{-1}$): 275(28 000), 485(88), 550(188), 650(250).

2.3.5. Preparation of $\text{PPh}_4[\text{Fe}^{\text{III}}\text{Cl}_4]$ (**5**)

$\text{FeCl}_3 \cdot 6\text{H}_2\text{O}$ (0.14 g; 0.50 mmol) was dissolved in 20 mL of 6 M aqueous HCl solution and stirred. Then 0.19 g (0.50 mmol) of PPh_4Cl dissolved in 0.5 mL of water was added to the above solu-

tion. A yellow solid separated, collected by filtration and washed with 4 M HCl solution. The product was then dried in vacuo and purified by recrystallization from methanol. *Anal. Calc.* for $\text{C}_{24}\text{H}_{20}\text{P}\text{Cl}_4\text{Fe}$: C, 53.67; H, 3.76; P, 5.77; Cl, 26.40; Fe, 10.40. *Found*: C, 53.3; H, 3.7; P, 6.0; Fe, 10.3; Cl, 27.0%. IR (KBr disc cm^{-1}): 3050(w), 1580(w), 1520(s), 1440(s), 1340(m), 1310(w), 1200(w), 1175(w), 1100(s), 1020(w), 1000(w), 920(w), 750(m), 730(s), 690(s), 530(s), 390(s), 310(w). UV-Vis [$\lambda_{\text{max}}/\text{nm}$ ($\epsilon/\text{M}^{-1}\text{cm}^{-1}$): 361(6735), 312(6405), 275(7610), 268(8535), 262(7510).

2.4. Crystal structure determination of **1**, **3** and **4**

Compound 1: A deep green crystal of dimensions, $0.40 \times 0.20 \times 0.08 \text{ mm}^3$, was mounted with Paratone-N oil (Hampton Research) coating. X-ray intensity data were collected at 296 K on a Bruker-Nonius X8-APEX2 CCD area-detector diffractometer using Mo $K\alpha$ radiation ($\lambda_{\text{max}} = 0.71073 \text{ \AA}$). Six sets of narrow data frames (10 s per frame) were collected at different values of θ for 5 and 1 initial value of ϕ and ω , respectively, using 0.5° increments of ϕ or ω . Data reduction was accomplished using SAINT V7.03 [31]. The substantial redundancy in data allowed a semi-empirical absorption correction (SADABS V2.10) [34] to be applied, on the basis of multiple measurements of equivalent reflections. The structure was solved by direct methods, developed by successive difference Fourier syntheses, and refined by full-matrix least-squares on all F^2 data using SHELXL V6.14 [35]. Hydrogen atoms were included in calculated positions and allowed to ride on their parent atoms. (**3**). A black crystal of dimensions $0.40 \times 0.30 \times 0.25 \text{ mm}^3$ was selected for indexing and intensity data collection. Measurements were carried out on a Siemens SMART three circle diffractometer equipped with a CCD bi-dimensional detector. The crystal to detector distance was 45 mm allowing the data collection up to 20–65°. An empirical absorption correction was applied using SADABS Program [36] based on the Blessing method [37]. The structure was solved by direct methods followed by Fourier difference syntheses using the SHELXL package [38]. All atoms except hydrogen atoms, C_9 and C_{10} carbon atoms, were anisotropically refined. Hydrogen atoms were refined with geometrical constraints **4**. A black crystal of dimension $0.10 \times 0.08 \times 0.06 \text{ mm}^3$ was isolated for intensity data collection. Single crystal diffraction data were collected on a Nonius Kappa CCD diffractometer at 298 K (λ (Mo $K\alpha$) = 0.71073 Å). The structures were solved by direct methods and refined by full-matrix least-squares on F^2 values using SHELXL-97 [39]. Selected crystallographic data together with the refinement details of compounds **1**, **3** and **4** are given in Table 1.

3. Results and discussion

3.1. Synthetic aspects

Since dppe was used as one of the ligands, a non-aqueous medium was necessary for the synthetic protocol in general and $\text{FeCl}_2 \cdot 4\text{H}_2\text{O}$ or $\text{FeCl}_3 \cdot 4\text{H}_2\text{O}$ were chosen as the starting materials. The appropriate iron salt and two equivalents of Na-DEDTC or Na-ETXANT were taken in ethanol, and dppe in dichloromethane, to obtain the products **1** and **2** as described in Section 2. If pure $\text{FeCl}_2 \cdot n\text{H}_2\text{O}$ is not available, $\text{FeCl}_3 \cdot n\text{H}_2\text{O}$ may also be used but in that case ascorbic acid must be used to reduce Fe^{III} to Fe^{II} for obtaining **1** and **2**. When saturated aqueous solution of $\text{NH}_2\text{OH} \cdot \text{HCl}$ in presence of 2 drops of concentrated HCl was used as reducing agent for Fe^{III} , the resulting solution on experimental work up generated a species, $[\text{Fe}^{\text{III}}(\text{dppe})(\text{DEDTC})_2]\text{Fe}^{\text{III}}\text{Cl}_4$ (**3**), where FeCl_4^- is the counter anion for the monocationic Fe^{III} complex while with ETXANT the Fe^{II} derivative $[\text{Fe}^{\text{II}}(\text{ETXANT})_2(\text{dppe})]$ (**2**) was obtained as the reaction product. Compound **3** on anion

Table 1Selected crystallographic data together with the refinement details are given for the compounds **1**, **3** and **4**.

	1	3	4
Empirical formula	C ₃₇ H ₄₆ N ₂ P ₂ S ₄ Cl ₂ Fe	C ₃₆ H ₄₄ N ₂ P ₂ S ₄ Cl ₄ Fe ₂	C ₆₀ H ₆₄ N ₂ P ₂ S ₄ BFe
Formula weight	835.69	948.41	1070.01
a (Å)	10.479(4)	19.0170(9)	11.706(1)
b (Å)	11.8234(6)	11.7288(5)	18.517(2)
c (Å)	18.0164(9)	20.1715(9)	26.747(3)
α (°)	71.378(2)	90	99.95(4)
β (°)	78.843(2)	101.2740(10)	99.48(4)
γ (°)	81.354(2)	90	95.56(5)
V (Å ³)	2065.9(1)	4412.4(3)	5585.5(1)
Z	2	4	2
Crystal System	triclinic	monoclinic	triclinic
Space group	P $\bar{1}$	P2 _{1/n}	P $\bar{1}$
ρ _{calc} (g/cm ³)	1.343	1.428	1.273
μ (Mo Kα) (mm ⁻¹) λ (Å)	0.71069	0.71073	0.71073
T (K)	296	296	298
Crystal size	0.40 × 0.20 × 0.08	0.40 × 0.30 × 0.25	0.10 × 0.08 × 0.06
μ (mm ⁻¹)	0.802	1.189	0.517
θ Limits (°)	1.21–30.11	1.35–25	2.07–26.37
Number of data collected	63 947	22 667	44 847
Number of unique data	12056	7754	22851
Number of data used for refinement (I) > 0(F _o) ²	8780	3611	11900
Goodness-of-fit (GOF) on F ²	1.092	0.933	1.024
R ₁ ^a (F _o)	0.0625	0.0612	0.0651
WR ₂ ^b (F _o) ²	0.1528	0.1270	0.1783

$$^a R_1 = \sum ||F_o| - |F_c|| / \sum |F_o|$$

$$^b WR_2 = \sqrt{\sum [W(F_o^2 - F_c^2)]^2 / \sum [W(F_o^2)]^2}$$

metathesis with NaBPh₄ in ethanolic medium gave [Fe^{III}(dppe)(DEDTC)₂]BPh₄ (**4**). The PPh₄ salt of the well-known FeCl₄⁻ (seems as yet unreported), was obtained quite easily as PPh₄[FeCl₄] (**5**). Compounds **4** and **5** were synthesized and characterized insofar as the measurement of magnetic susceptibility and Mössbauer spectroscopy of these two compounds were necessary for explaining the magnetic and Mössbauer behavior of the cation of **3**.

3.2. General characterization

While compounds **3**, **4** and **5** are 1:1 electrolytes (observed molar conductance, $\Lambda_M = 150 \text{ ohm}^{-1} \text{ cm}^2 \text{ mol}^{-1}$) in acetonitrile [40] **1** and **2** are non-electrolytes, as expected. The molecular weight data indicate that the compounds are discrete molecules in CH₃CN at room temperature. A strong vibrational band appears at 1478 cm⁻¹ in the IR spectrum of Na-DEDTC · 3H₂O which can be assigned as ν(CN) (here thiouride band) vibration which is very much characteristic of this ligand [41,42]. In complexes **1**, **3** and **4** this band appears at a higher wave number region (see Section 2) due to enhanced double bond character of the C–N bond after metal coordination. The ν(CS) stretch in the three DEDTC complexes is uniquely represented by a medium intensity band at 1000 cm⁻¹. Occurrence of no other DEDTC band between the spectral region 1420 and 1480 cm⁻¹ indicates that in all the three complexes DEDTC functions as a bidentate ligand [42]. Absorption due to ν(NC₂, ethyl C) of free DEDTC (1200 cm⁻¹) suffers a lower wave number shift (ca. 150 cm⁻¹) in all the three DEDTC complexes. The complex **2** is characterized by ν(C–O–C=S) vibration at 1030(w), 1180(w), 1080(w), 1210(s) which is typical for the bidentate xanthate ligand [43,44]. In all the complexes the strong to medium intensity bands around 1500, 1440, 1120, 750, 725, 700 and 520 cm⁻¹ appear due to the dppe vibrations. The ν(Fe^{II}–P) vibration [45] in **1** and **2** occurs at 330 cm⁻¹, while the same in **3** and **4** appears around 260 cm⁻¹ indicating that the Fe^{III}–P bond is much weaker than the corresponding Fe^{II}–P bond. The (Fe^{II}–S) vibrations [46] in all the DEDTC complexes appear at 350 cm⁻¹ but in xanthate complex at 380 cm⁻¹ suggesting that the ETXANT is a stronger ligand than DEDTC in Fe (III) as well as Fe (II) complexes. In compound **3**, the ν(Fe–Cl) vibration oc-

curs as a very prominent band at 390 cm⁻¹ which is split as a shoulder at 380 cm⁻¹ due to the isotopic factor involved in ³⁵Cl and ³⁷Cl. This is considered diagnostic [47,48] for T_d FeCl₄⁻ otherwise absent in **1**, **2** and **4** but present in **3**, besides occurring as a strong band in **5**. Compound **5** shows five electronic spectral bands of which those at 361 nm ($\epsilon = 6735 \text{ M}^{-1} \text{ cm}^{-1}$) and at 312 nm ($\epsilon = 6405 \text{ M}^{-1} \text{ cm}^{-1}$) are due to the Cl⁻ → Fe (III) LMCT transition and the other three are due to the PPh₄⁺ ion. Complex **3** shows the above transition at 360 nm ($\epsilon = 3400$) whereas the higher wave length bands are due to ligand field transitions of strong field Fe (III), namely, ²T_{2g} → ²T_{1g}, ²T_{2g} → ²A_{2g} and ²T_{2g} → ²E_g (Fig. 1, these terms originated from the ²I field free ionic term of the Fe³⁺ ion [49]). Compound **4** also shows similar high wavelength d–d bands (Fig. 1) with high ϵ (M⁻¹ cm⁻¹) in both the complexes (see Section 2) but obviously no band at 360 nm (Fig. 1). The diamagnetic complexes **1** and **2** show two bands in the visible region (see Section 2).

3.3. Proton NMR spectroscopy of **2**

The proton NMR of **2**, whose structure is expected to be similar to that of **1** (two DEDTC are substituted by two ETXANT) constitutes a triplet ($J = 6 \text{ Hz}$) at $\delta = 0.9 \text{ ppm}$ (6H) due to the methyl groups of the two xanthate ligands, a quartet ($J = 6 \text{ Hz}$) at $\delta = 3.9 \text{ ppm}$ (4H) due to two CH₂ groups of the two xanthate ligands and a singlet at $\delta = 2.6 \text{ ppm}$ (4H) due to four CH₂ protons of the dppe ligand. The appearance of a single proton signal for two CH₂ groups of the dppe ligand is a consequence of the fact that a C₂ axis of the molecule **2** bisects the C–C bond of the two CH₂ groups establishing a magnetic equivalence of all the four protons of the ethene residue. This supports the structural similarity between the complexes **1** and **2**.

Mass spectrometry: (a) *Electron impact mass spectrometry.* The peaks observed in **2** are at $m/e = 89$ (C₂H₅OS) 108 (PPh₂), 121 (EtOCS₂), 262 (Ph₃P), 370 (Ph₂P–PPh₂) 398 (dppe) and 269 (probably corresponding to [Fe^{II}(COS₂) (ETXANT)]) [26]. As usual the satellite peaks are due to the isotopic compositions of sulfur, carbon, nitrogen, etc, as may be the case here.

(b) *FAB (Fast Atom Bombardment) mass spectrometry.* Besides X-ray crystallography complexes **1** and **3** have been further

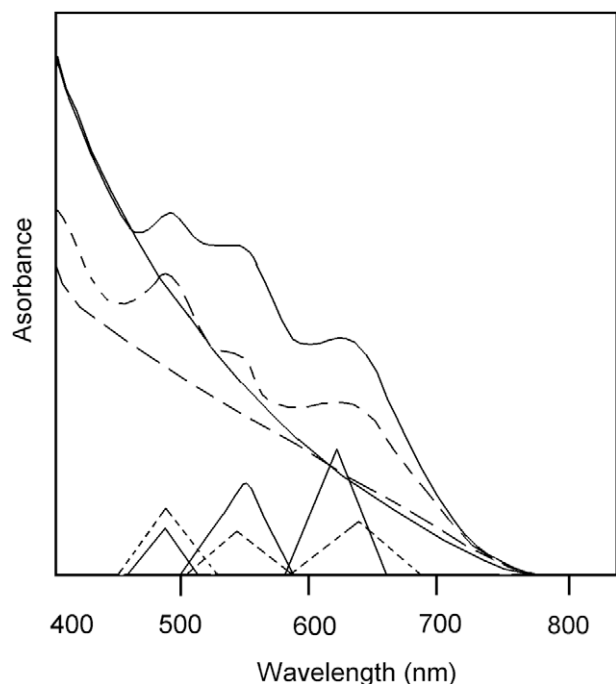


Fig. 1. Electronic Spectra (Gaussian Analyzed) of **3** (----) and **4** (—).

characterized using FAB mass spectroscopy. In the positive ion mode **1** shows a distinct and intense molecular ion peak at $m/z = 750$ amu $[\text{Fe}(\text{Ph}_2\text{PCH}_2\text{CH}_2\text{PPh}_2)(\text{C}_2\text{H}_5)_2\text{NCS}_2]_2^+$. Besides this, other peaks observed at $m/z = 602, 399, 352$ and 204 amu correspond to $[\text{Fe}(\text{dppe})(\text{DEDTC})]^+$, $(\text{dppe})^+$, $[\text{Fe}(\text{DEDTC})_2]^+$ and $[\text{Fe}(\text{DEDTC})]^+$ ions, respectively. In the negative ion mode the peak at $m/z = 148$ and 204 amu are due to $(\text{DEDTC})^-$ and $[\text{Fe}(\text{DEDTC})]^-$ ions, respectively. In complex **3** an intense molecular ion peak is observed at $m/z = 950$ amu for the $[\{\text{Fe}(\text{dppe})(\text{DEDTC})_2\}\text{FeCl}_4]^+$ ion in the positive ion mode. In the negative ion mode a distinct and intense peak at $m/z = 198$ amu is obtained for the $[\text{FeCl}_4]^-$ ion, otherwise absent in **1**.

3.4. X-ray photoelectron spectroscopy

Inner electron binding energies of S2p, Fe2p_{1/2} as recorded in Table 2, for **1** and **2** signify that as usual ETXANT is a stronger ligand than DEDTC, since the S2p binding energy of the coordinated ETXANT ligand has a slightly higher value (eV) than that of coordinated DEDTC indicating that a greater amount of electron density of the xanthate ligand is transferred to the metal ion compared to that of the DEDTC ligand. On the other hand the appropriate binding energies from XPS results of two iron 2p multiplets are higher in energy for the complex **1** than for complex **2**, implying that electron density enrichment of the Fe2p orbital in **1** is lower than in **2** due to the weaker S-coordination in the former than that of the later. The S2p binding energy of the Fe^{III} complex, **4** is a bit

Table 2
Relevant inner electron binding energies of S2p and Fe2p electrons of **1**, **2** and **4** from XPS results.

Complex	Binding energy (eV)		
	S2p	Fe2p _{3/2}	Fe2p _{1/2}
$[\text{Fe}^{\text{II}}(\text{DEDTC})_2(\text{dppe})]\text{CH}_2\text{Cl}_2$ (1)	162.5	709.3	724.5
$[\text{Fe}^{\text{II}}(\text{ETXANT})_2(\text{dppe})]$ (2)	163.0	708.5	722.0
$[\text{Fe}^{\text{III}}(\text{DEDTC})_2(\text{dppe})]\text{BPh}_4$ (3)	163.8	707.4	720.1

higher and Fe2p binding energies lower than those of the Fe^{II} complexes. This is clear indication that the DEDTC ligand binds more strongly to the Fe^{III} than to Fe^{II}. For all practical purposes it should be borne in mind that π -acidity of DEDTC and ETXANT are negligible.

3.5. Molecular structure of **1**, **3** and **4**

The crystal of compound **1** contains discrete monomeric units of $[\text{Fe}(\text{dppe})(\text{DEDTC})_2]$ and a molecule of CH_2Cl_2 per unit, held in the lattice. A view of compound **1** is shown in Fig. 2. A packing diagram (Fig. 3) showing of four unit cells in bc plane exhibiting the lattice held CH_2Cl_2 one in each formula unit. The closest approach of C–H hydrogens towards the chlorine atoms of CH_2Cl_2 does not show any H-bonding (as examined by using a MERCURY software) interaction. Structure of the cationic part of complex **3** $[\text{Fe}(\text{dppe})(\text{DEDTC})_2]^+$ is analogous to compound **1**, but complex **3** has another tetrahedral Fe (III) center, FeCl_4^- , held in the lattice. A view of the cationic part of **3** is shown in Fig. 4. The crystal structure of compound **4** consists of the cationic $[\text{Fe}(\text{dppe})(\text{DEDTC})_2]^+$ complex associated with BPh_4^- . Two cation–anion moieties are found in the asymmetric crystal unit. A view of the cationic units of $[\text{Fe}(\text{dppe})(\text{DEDTC})_2]\text{BPh}_4$ (**4**) which are non-enantiomers is shown in Fig. 5. A view of the asymmetric unit with the atom numbering information scheme is provided as Supporting material (Fig. SI-2). The molecular structure of the cationic unit of $[\text{Fe}(\text{dppe})(\text{DEDTC})_2]^+$ for both **3** and **4** as well as the two molecules in **4** are very similar (see Table 3) and the values of angles around the atoms are shown in Table 4. It is obvious from Fig. 3 that the very small differences of bond lengths and inter-bond angles (Table 4) are due to the nature of crystal packing. Figs. 2–4 and the bond length and bond angle data in Tables 3 and 4 indicate that the geometry around the Fe (II) and Fe (III) centers can be best described as distorted octahedral. The Fe (III)–P distances are remarkably longer than those in Fe (II)–P bond lengths as shown in Table 3, in contrast Fe (III)–S are shorter than those in Fe (II)–S bond lengths Iron (II) being a less hard (borderline) acceptor than Iron (III), the Fe^{III}–P bond distances in **3** and **4** are obviously (Table 3) longer than those in **1**, since phosphorus donors are moderately good π -accepting and soft donor [for HSAB principles and details see Refs. [50,51]. Sulfur atom belonging to the period 3 of the periodic table is labeled as soft donor because in principle it can use its 3d orbitals for back acceptance of metal electrons but the phosphorus donors are always

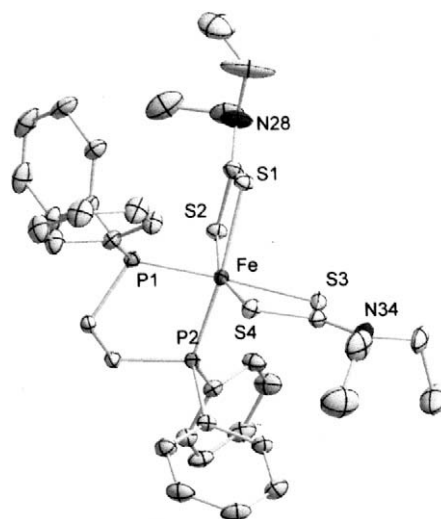


Fig. 2. View of $[\text{Fe}(\text{dppe})(\text{DEDTC})_2]$ (**1**). Displacement ellipsoids are scaled to enclose 30% probability levels. Hydrogen atoms are not represented.

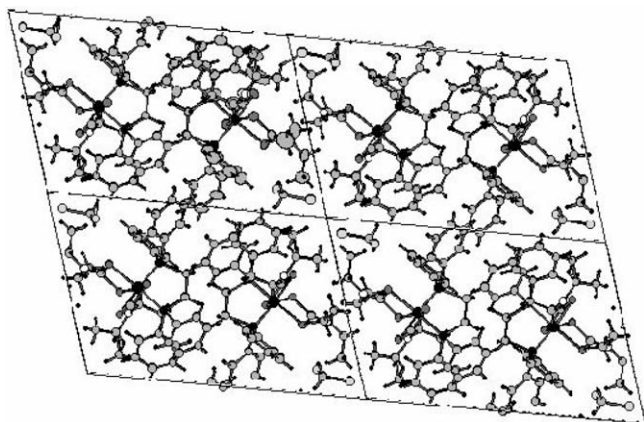


Fig. 3. The packing diagram for compound **1**, [Fe(dppe)(DEDTC)₂] showing the lattice held solvent molecules.

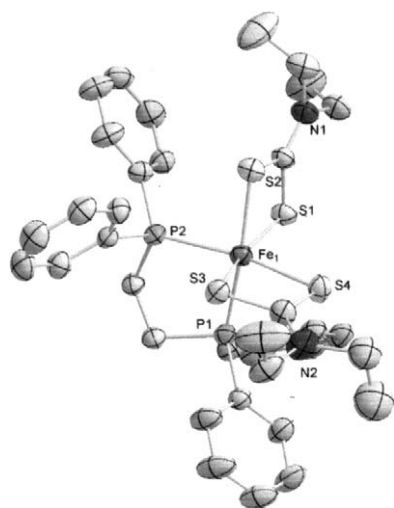


Fig. 4. View of the cationic moiety of [Fe(dppe)(DEDTC)₂]FeCl₄ (**3**). Displacement ellipsoids are scaled to enclose 30% probability levels. Hydrogen atoms are not represented.

better π -acids than the S-donors. This explains the nature of iron–phosphorous and iron–sulfur bond lengths. However, the Fe–S distances observed here are a bit more prominent [52] since the Fe^{II}–S bond lengths are a part of the molecular species **1** which is neutral but that of Fe^{III}–S belongs to a molecule which carries a positive charge. Pauling's electro-neutrality principle suggests that in **3** the iron (III) ion will get a good share of the 1+ charge rendering it electron poorer enough to enforce S-atoms of DEDTC to make a more effective overlap with the said Fe^{III} empty $d\sigma$ orbitals than that furnished with neutral Fe^{II} system, in **1**.

3.6. Magnetic properties

The temperature dependence of the molar magnetic susceptibility, χ_M , for compounds **3–5** have been investigated in the temperature range 2–300 K. The results are plotted as $\chi_M T$ versus T in Figs. 6–8 together with the field dependence of their magnetization at 2 K.

[Fe(dppe)(DEDTC)₂][FeCl₄] (**3**). The $\chi_M T$ for compound **3** between 300 and 50 K remains invariant with a value of 4.91 cm³ K mol⁻¹. This value is in good agreement with that anticipated for two non-interacting spins with $S = 5/2$ and $S = 1/2$ (4.75 cm³ K mol⁻¹ assuming $g = 2$). These spins are attributed respectively to the T_d Fe (III) unit, [FeCl₄]⁻, and to the octahedral low-spin Fe (III) moiety,

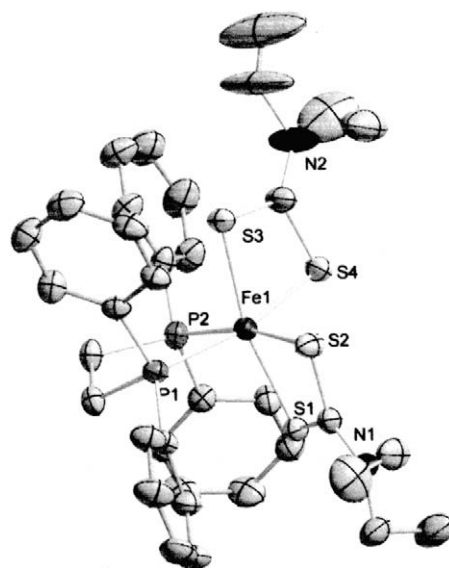


Fig. 5. View of the cationic moiety of [Fe(dppe)(DEDTC)₂]BPh₄ (**4**). Displacement ellipsoids are scaled to enclose 30% probability levels. Hydrogen atoms are not represented.

Table 3
Main bond distances (Å) for compounds **1**, **3** and **4**.

	1	3	4
Fe–P ₂	2.1945(8)	2.3064(18)	2.3088(1) 2.3056(12)
Fe–P ₁	2.1942(8)	2.3178(18)	2.3164(13) 2.3147(12)
Fe–S ₂	2.3110(9)	2.2906(18)	2.2875(13) 2.2875(12)
Fe–S ₄	2.3083(9)	2.2880(19)	2.2898(13) 2.2826(12)
Fe–S ₃	2.3586(9)	2.2981(17)	2.3024(13) 2.3022(12)
Fe–S ₁	2.3571(9)	2.2937(17)	2.3044(13) 2.3071(13)

Table 4
Main bond angles (°) for compounds **1**, **3** and **4**.

1	3	4
S ₄ –Fe–S ₂ 162.94(4)	S ₁ –Fe–S ₃ 165.88(7)	S ₃ –Fe ₁ –S ₁ 165.65(5)
		S ₅ –Fe ₂ –S ₈ 164.08(5)
P ₂ –Fe–S ₁ 170.18(3)	S ₄ –Fe–P ₂ 169.92(7)	S ₂ –Fe ₁ –P ₂ 168.02(5)
		S ₇ –Fe ₂ –P ₄ 169.32(5)
P ₁ –Fe–S ₃ 171.49(4)	S ₂ –Fe–P ₁ 168.15(7)	S ₄ –Fe ₁ –P ₁ 167.65(5)
		S ₆ –Fe ₂ –P ₃ 167.19(5)

[Fe(dppe)(DEDTC)]⁺. Below 50 K, $\chi_M T$ increases and reaches a value of 5.55 cm³ K mol⁻¹ at 2 K (vide infra for discussion). The field dependence of the magnetization at 2 K for this compound is depicted as inset in Fig. 6.

For the highest field investigated, the magnetization tends to a saturation value of 6 μ_B in agreement with the contribution of six unpaired electrons.

[Fe(dppe)(DEDTC)₂]BPh₄ (**4**). For this compound the value of $\chi_M T$ between 300 and 60 K is constant and amounts to 0.46 cm³ K mol⁻¹ in agreement with low-spin Fe (III) as in **3**. Below 60 K $\chi_M T$ decreases rapidly and reaches 0.21 cm³ K mol⁻¹ for 2 K, suggesting the occurrence of weak antiferromagnetic interactions among the spin carriers. This is confirmed by the magnetization curve (Fig. 7) recorded at 2 K which reaches just 0.61 μ_B in an applied field of 5T.

PPh₄[FeCl₄] (**5**): Compound **5** exhibits a paramagnetic behavior down to very low temperature with a $\chi_M T$ value of 4.40 cm³ K mol⁻¹ in agreement with a $S = 5/2$ spin ground state

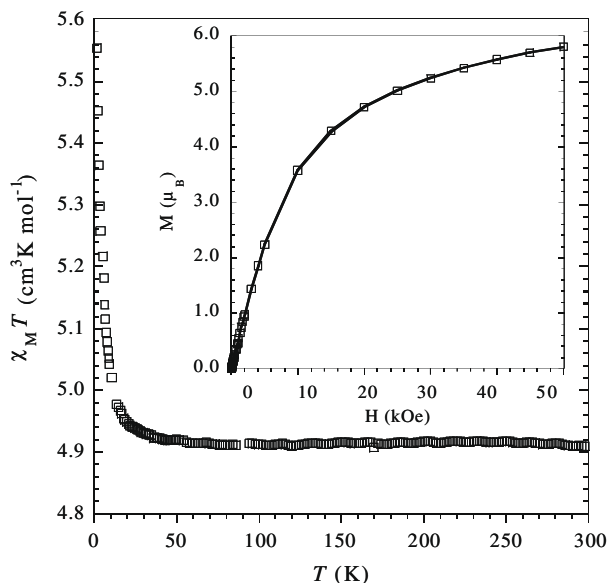


Fig. 6. Temperature dependence of $\chi_M T$ for $[\text{Fe}(\text{dppe})(\text{DEDTC})_2]\text{FeCl}_4$ (**3**). Inset: Field dependence of the magnetization at 2 K.

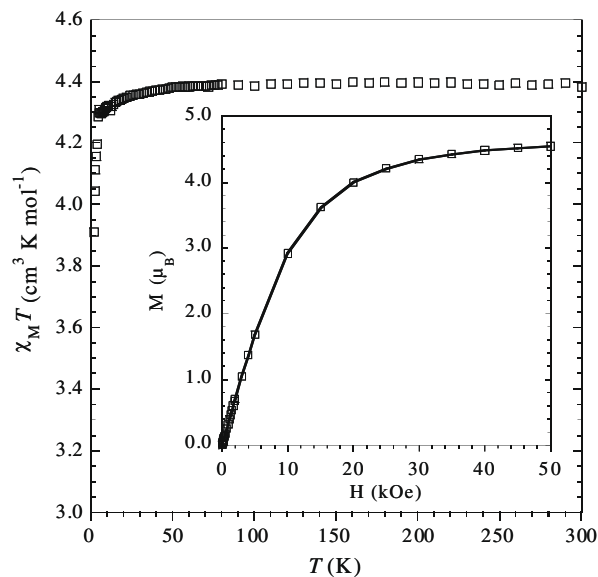


Fig. 8. Temperature dependence of $\chi_M T$ for $\text{PPh}_4\text{FeCl}_4$ (**5**). Inset: Field dependence of the magnetization at 2 K.

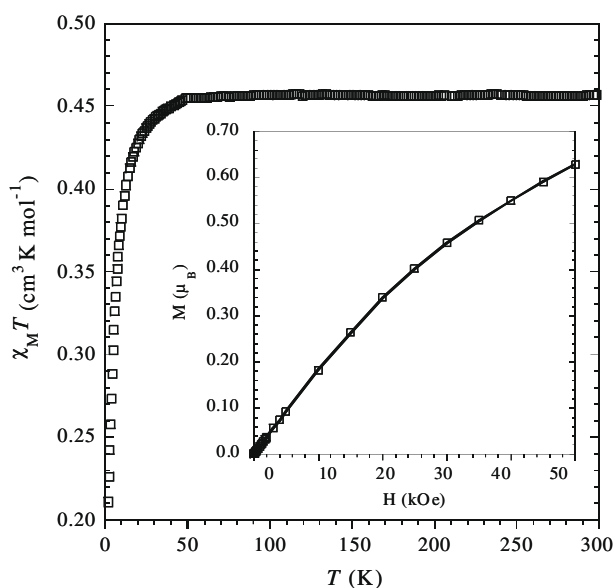


Fig. 7. Temperature dependence of $\chi_M T$ for $[\text{Fe}(\text{dppe})(\text{DEDTC})_2]\text{BPh}_4$ (**4**). Inset: Field dependence of the magnetization at 2 K.

(Fig. 8). This is also supported by the field dependence of the magnetization that tends to $5 \mu_B$ for the highest field investigated. These data are consistent with those reported for related $[\text{FeCl}_4]^-$ salts [53].

The magnetic behavior for compounds **3** and **4** clearly show that Fe (III) has low-spin with $S = 1/2$ in $[\text{Fe}(\text{dppe})(\text{DEDTC})_2]^+$. Moreover, no evidence was found for a crossover to a higher spin state with temperature as often observed for related Fe–DEDTC complexes [19,54]. This low-spin state can be attributed to the octahedral coordination sphere of Fe (III), which excludes the possibility for intermediate spin state $S = 3/2$, because of a stronger ligand field induced by the dppe ligand. It is important to note that for the $[\text{Fe}(\text{dppe})(\text{DEDTC})_2]^+$ cation and the $[\text{FeCl}_4]^-$ anion the magnetic behaviors are the same whether these species are combined as in compound **3** or taken individually in salts with non-magnetic

counter-ions. Thus the magnetic behavior of $[\text{Fe}(\text{dppe})(\text{DEDTC})_2]\text{FeCl}_4$ (**3**) in the temperature domain 40–300 K is simply the sum of the contribution of each Fe moiety in its ligand surrounding. This is also confirmed by the Mössbauer studies (vide infra). However, the magnetic behavior of compound **3** is characterized by an increase of $\chi_M T$ below 20 K, which is found neither for **4** nor for **5**.

Two hypotheses can be invoked to explain this increase. The first possibility is that the spin state for cation of **3** is modified at low temperature. This could result from a structural evolution affecting the octahedral coordination sphere and subsequently the ligand field strength, allowing a crossover from $S = 1/2$ spin to a larger spin state. However, no evidence for such a process is detected by Mössbauer spectroscopy (see later). The second possibility is the occurrence of weak intermolecular ferromagnetic interaction among the Fe centers. The structural data for compound **3** permit to identify a short S–S contact ($\text{S}2 \cdots \text{S}2$, 4.03(11) Å; $\text{S}7 \cdots \text{S}7$, 4.19(12) Å) between two adjacent $[\text{Fe}(\text{dppe})(\text{DEDTC})_2]^+$ cations in the crystal lattice (Fig. 9). Such a contact can propagate weak exchange interaction between the magnetic centers. In the present case, these contacts lead to ferromagnetic interactions. This latter hypothesis is more realistic and is supported by the ferromagnetic ordering found for $[\text{Fe}(\text{DEDTC})_2\text{Cl}]$ [55].

3.7. Magnetic behavior of the diamagnetic compound $[\text{Fe}(\text{dppe})(\text{DEDTC})_2]$ (**1**)

Recording the variable temperature magnetic moment of the low-spin diamagnetic compound **1** in the temperature range 400–2 K shows typical diamagnetic behavior with out any spin crossover with T . This was quite expected since the compound is diamagnetic at 298 K and it is almost a ‘truth’ that ‘diamagnetism is independent of temperature’. There is no way that it can acquire paramagnetism at lower temperature because energies involved are insignificant enough to cause any spin decoupling. This statement will remain valid even if some phase transition due to structure distortion occurs [22] and occurrence of that too is very remote at lower temperature. At the higher temperature 300–400 K $\chi_M T$ versus T plot (given as Fig. SI-3) for the compound shows a little deviation which is due to the oxidation of Fe^{II} to Fe^{III}

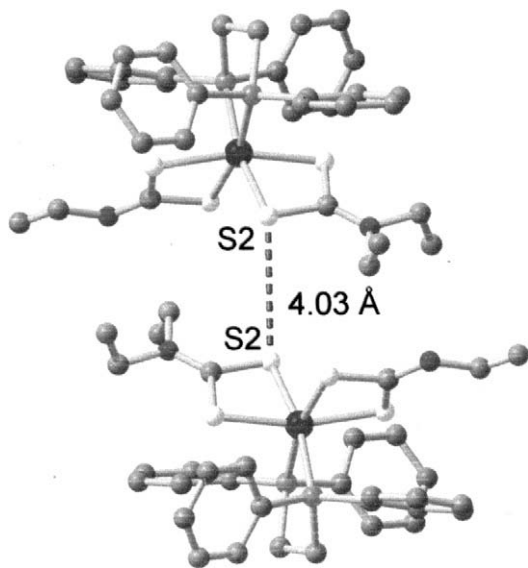


Fig. 9. View of the short S...S contact (dotted line) existing between the cationic $[\text{Fe}(\text{dppe})(\text{DEDTC})_2]^+$ units of **3** in the solid.

which occurs almost in all cases studied, even by diluting the Fe^{II} compound via solid solution formation [56]. The compound starts decomposing above 400 K. Strictly speaking a very little Fe^{III} impurity cannot be ruled out from $\chi_{\text{M}}T$ ($\text{cm}^3 \text{K mol}^{-1}$) versus temperature (400–298 K) plot, which has been explained by many authors working with other Fe (II) systems.

3.8. Mössbauer spectroscopy for compounds **3**, **4**, and **5**

In order to evaluate the spin states of these Fe derivatives and their possible evolution with temperature we have recorded the

Mössbauer spectra for compounds **3**, **4**, and **5** at 293 K and at 4.2 K. Results are displayed in Fig. 10 and Tables 5–7.

Behavior at 293 K: For all three compounds, the spectra obtained at 293 K have been analyzed by considering the contributions from one octahedral (O_h) iron site (with $S = 1/2$) and from a tetrahedral (T_d) Fe site (with $S = 5/2$). For $[\text{Fe}^{\text{III}}(\text{dppe})(\text{DEDTC})_2]\text{FeCl}_4$ **3** a 1:1 distribution of O_h and T_d sites is anticipated, but a discrepancy is found (65:35). It can be stressed that the purity of the microcrystalline powder used for Mössbauer studies was checked by powder X-ray diffraction. The experimental diffractogram matches with the diffractogram calculated with the crystal data of the structure of **3** (Fig. SI-4) confirming that the sample corresponds to the known (structurally confirmed) compound and does not contain detectable amounts (more than ca. 5%) of other species. So, the reason for this discrepancy is not obvious at present. The above ratio was different for an aged sample (Table 5). In Fig. 10 are compared the spectra obtained initially for compound **3** and for the same sample several months later (aged). It appears clearly that aging leads to an increase of the contribution attributed to T_d sites with respect to the octahedral (O_h) Fe center. This suggests that the evolution of compound **3** involves a modification of the coordination sphere of the $\{\text{Fe}(\text{DEDTC})_2(\text{dppe})\}$ unit. For $[\text{Fe}^{\text{III}}(\text{dppe})(\text{DEDTC})_2]\text{BPh}_4$ (**4**) the data confirm the main occurrence of the expected O_h site but some T_d sites are also found. In view of qualitative tests conducted for Cl^- ion showing negative response, we attribute the presence of T_d sites in **4** to the decomposition product of the O_h Fe center as evidenced above. Finally, data and analysis for $\text{PPh}_4[\text{FeCl}_4]$ (**5**) are in agreement with the anticipated parameters for a T_d Fe (III) center with $S = 5/2$. A very good fit has been obtained when considering the contribution of an O_h impurity but its amount (<3%) clearly underlines the purity of the sample.

Behavior at 4.2 K: The experimental and curve fitted spectra at 4.2 K for compounds **3**–**5** are depicted in Fig. 10. Based on the data obtained at 293 K, a first refinement with a Lorentzian peak profile yielded rather large peak width values. Therefore the spectra have

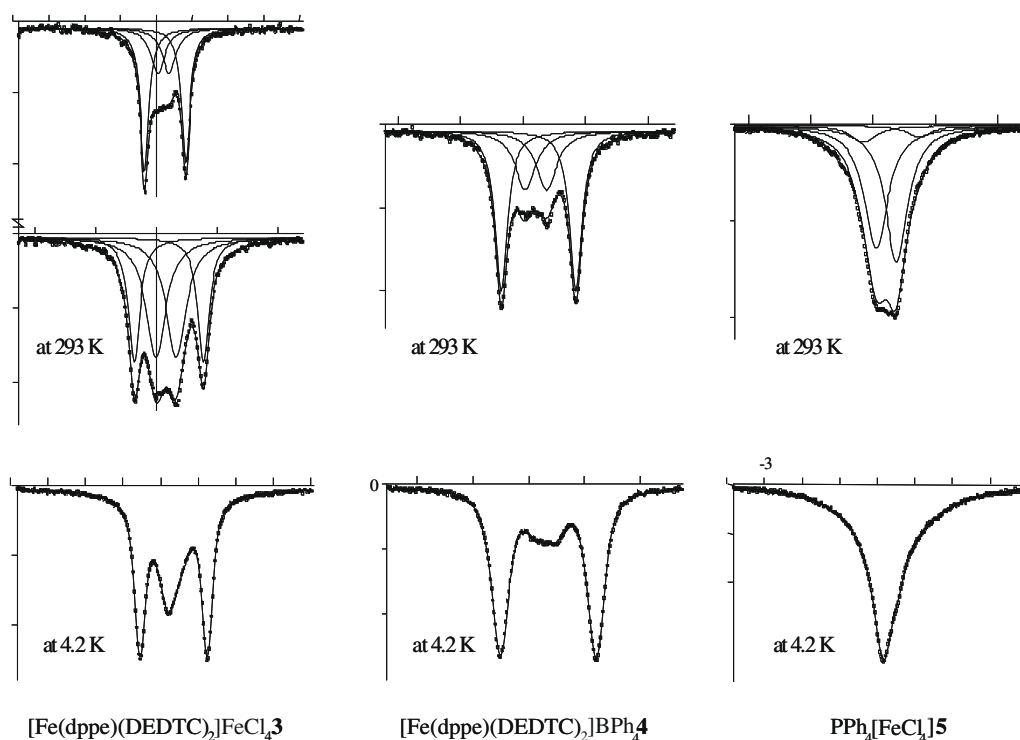


Fig. 10. Experimental (\square) and simulated (---) Mössbauer spectra for (left) compound **3**, (middle) compound **4**, and (right) compound **5** at respectively, (top) 293 K and (bottom) 4.2 K.

Table 5

Hyperfine parameters at 293 K for compounds **3**, **4**, and **5** deduced from curve simulation by considering the contributions from one octahedral site (1) and from one tetrahedral site (2).

Fe site	δ (mm s ⁻¹) ^a	Δ (mm s ⁻¹) ^b	Γ (mm s ⁻¹) ^c	%
Compound 3 (initial)				
1 (O _h)	0.265(3)	1.150(3)	0.284(4)	65
2 (T _d)	0.215(12)	0.312(12)	0.466(30)	35
Compound 3 (aged)				
1 (O _h)	0.263(4)	1.142(4)	0.225(3)	37
2 (T _d)	0.217(7)	0.332(7)	0.393(6)	63
Compound 4				
1 (O _h)	0.260(1)	1.202(1)	0.235(3)	62
2 (T _d)	0.218(14)	0.340(14)	0.40(1)	38
Compound 5				
1 (O _h)	0.25(22)	1.60(22)	0.49(13)	3
2 (T _d)	0.216(4)	0.340(4)	0.426(5)	97

^a δ = isomer shift.

^b Δ = quadrupole splitting.

^c Γ = band width.

Table 6

Hyperfine parameters at 4.2 K for compounds **3**, **4**, and **5** deduced from curve simulation by considering distributions of quadrupole splitting (DIS1 and DIS3), and hyperfine fields (DIS2).

Distribution	δ (mm s ⁻¹) ^a	Δ (mm s ⁻¹) ^b	Γ (mm s ⁻¹) ^c	%	H (T) ^d
Compound 3					
DIS1	0.33		0.35	38	4.2
DIS2	0.37	1.75	0.22	52.0	
DIS3	0.21	0.39	0.30	10	
Compound 4					
DIS1	0.33		0.35	23	4.1
DIS2	0.37	1.72	0.22	68	
DIS3	0.21	1.39	0.30	9	
Compound 5					
DIS1	0.33		0.35	67	6.8
DIS2					
DIS3	0.21	0.37	0.25	33	

^a δ = isomer shift.

^b Δ = mean quadrupole splitting.

^c Γ = band width.

^d Mean hyperfine field.

Table 7

Population of octahedral and tetrahedral sites at 293 K and 4.2 K for compounds **3–5** deduced from spectra simulations.

	3	3 Aged	4	5
At 293 K				
O _h sites	65%	37%	62%	3%
T _d sites	35%	63%	38%	97%
At 4.2 K				
DIS2	52%		68%	0%
DIS1 + DIS3	48%		32%	100%

been analyzed by considering either one or two quadrupole splitting distributions and one hyperfine field distribution (see Section 2). The values for the chemical shifts allow for attributing each distribution to Fe (III) in two environments. Hence, distribution DIS2 concerns the Fe in O_h surrounding whereas DIS1 and DIS3 apply to T_d sites. Thus, for compounds **3** and **4**, two distributions of the quadrupole splitting (DIS2 and DIS3) have been considered as well as a hyperfine fields distribution (DIS1) whereas for compound **5** a hyperfine field distribution and only one quadrupole splitting distribution have been considered. A very good agreement of the

parameters deduced from the data of all compounds at 4.2 K is observed (Table 6). From the data of compound **5** at 293 K and 4.2 K we can conclude that the hyperfine parameters obtained at 4.2 K are those of the T_d Fe (III) center with $S = 5/2$ [57]. Distribution DIS1 corresponds to what is expected for Fe (III) in a four-ligand surrounding, the difference of isomer shift between 293 K ($\delta_{293} = 0.21$ mm s⁻¹) and 4.2 K ($\delta_{4.2} = 0.33$ mm s⁻¹) is due to a second order Doppler effect which leads to an increase of δ when T is lowered. Formally, DIS3 should correspond to a second Fe (III) site which however, is not detected at 293 K. Therefore, we suppose that this second site simply result from a geometrical distortion of the T_d FeCl₄⁻ unit at low temperature.

For compound **3** we get the two distributions (DIS1 and DIS3) found for **5** and a third contribution (DIS2), which is not perturbed by a magnetic exchange interaction. The hyperfine parameters associated to this latter distribution are attributed to the Fe (III) in octahedral surrounding, i.e. [Fe(DEDTC)₂(dppe)]⁺. As mentioned previously, the difference between the isomer shift found at 293 K ($\delta_{293} = 0.26$ mm s⁻¹) and that at 4.2 K for DIS2 ($\delta_{4.2} = 0.37$ mm s⁻¹) is due to the second order Doppler effect. For compound **4**, best analysis has been obtained when the same contributions as for compound **3** were considered; the results are very similar as far as hyperfine parameters are concerned. This confirms that compound **4** contains the expected O_h unit but also some amount of a tetrahedral component that can be attributed to sample aging.

The population obtained for the octahedral and tetrahedral sites both at 293 K and 4.2 K are summarized in Table 7. For compounds **4** and **5** the populations are found to be very similar at 293 K and 4.2 K, some deviation is observed for compound **3**. For the latter compounds, a 1:1 ratio between the O_h and T_d sites is found at 4.2 K but this ratio deviates significantly for the chemical composition at 293 K with 65% O_h sites. This discrepancy might be attributed to the Lamb Mössbauer parameters (f) for [Fe(DEDTC)₂(dppe)]⁺ and [FeCl₄]⁻ that could be very similar at 4.2 K but different at high temperature yielding populations much closer to reality at low temperature.

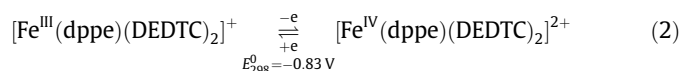
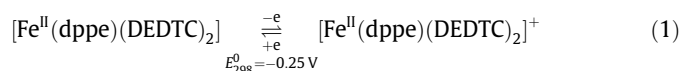
3.9. Mössbauer spectroscopy for **1**

The magnetic behavior discussed earlier (Section 3.7) is fully supported (100%) by the Mössbauer data (Fig. 11). The signal obtained (doublet 1) is in agreement with low-spin ($S = 0$) Fe^{II}, which overlaps with the simulated signal (doublet 1). A small amount of impurity, however, appears as doublet 2 (see also Fig. 11).

3.10. Electrochemical redox responsivity of DEDTC complexes

The cyclic voltammograms of the isolated complexes **1**, **3** and **4** have been recorded in acetonitrile/TEAP medium using Pt-wire working electrode. The results are summarized in Table 8 and the voltammograms in Fig. 12.

Comparing the cyclic voltammetric data as well as the voltammograms of complex **1** (Fig. 12A) with those of [Fe(DEDTC)₃] [25], it becomes apparent that two metal centered redox responses observed represent the electrochemical redox reactions shown in Eqs. (1) and (2) in 1.



However, a quantitative comparison of the above results with the potential of the redox cycle [Fe^{III}(DEDTC)₃] ⇌ [Fe^{IV}(DEDTC)₃], conveys that the substitution of one DEDTC-ligand by dppe the

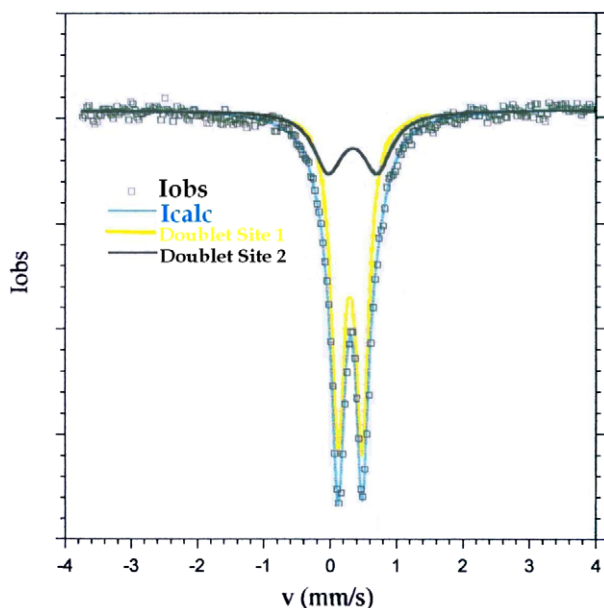


Fig. 11. Mössbauer spectra of the diamagnetic compound **1**, [Fe(dppe)(DEDTC)₂].

E_{298}^0 of the reaction undergoes remarkable increase insofar as the P–P donor is a reasonably strong π -acid. The M π L π -back donation reduces the metal electron density and hence further oxidation to metal center requires higher energy. Interestingly, the Fe^{III} complex cation, **3** having FeCl₄[−] as the counter anion exhibits three voltammetric cyclic responses (Fig. 12B). The redox steps for the cyclic responses in this case is shown as Eqs. (3)–(5). Surprisingly the oxidative response of **4** is irreversible and is assignable as Eq. (6) but the reductive response (Fe^{III} ⇌ Fe^{II}) is reversible (Eq. (7)).

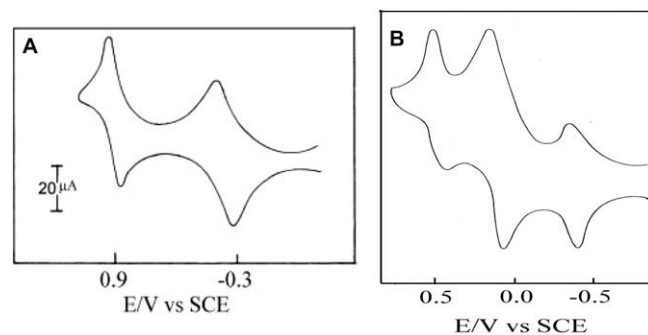
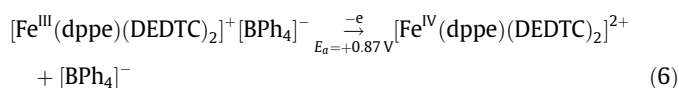
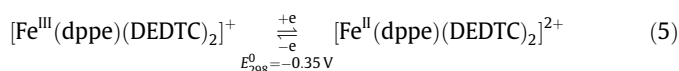
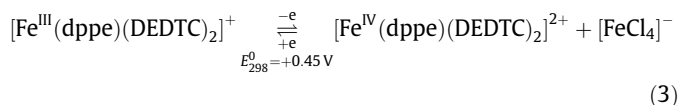
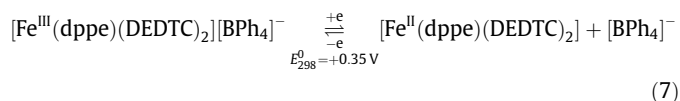
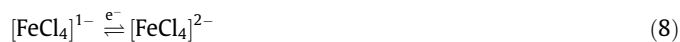


Fig. 12. (A and B) Cyclic voltammograms of compounds **1** and **4** in CH₃CN/TEAP medium at scan rate of 50 mV/s.



It is well known that various cationic iron (IV) complexes can be made by chemical and electrochemical oxidation of Fe (III) complexes [58]. Hence it is quite expected that all the complexes studied here will show a Fe^{III} ⇌ Fe^{IV} response, which is actually the case. Attention may be drawn to Eqs. (2) and (3) and the irreversible process represented by Eq. (6), which all represents the oxidation of the same complex ionic species. The difference lies in the Fe^{III} ⇌ Fe^{IV} potential as shown in Eq. (2) and the same cation associated with tetrahedral counter anions containing Fe^{III} in Eq. (3) and B^{III} in Eq. (6). An association of the counter ion is not responsible for the difference in electrode potential as can be seen from Eqs. (2) and (6). But in Eq. (3) we deal with the [FeS₄P₂]⁺ system associated with the [Fe^{III}Cl₄][−] counter anion and the electrode potential for the cyclic response is lower than that represented by Eqs. (2) and (6), although of course in (6) the represented response is acyclic.

In a dipolar solvent both two Fe^{III} centers of **3**, whose redox behavior is represented in Eq. (3), will be solvent clustered and electron transfer from clustered [Fe^{III}][−] to clustered [Fe^{III}]⁺ may slightly increase ($\Delta E^0 = E_C^0 - E_A^0$) the electron density of the positively charged iron center and it requires less energy (hence lower potential) for its oxidation to Fe^{IV}. Concisely in **1** and **4** (if we ignore the irreversibility of the oxidation reaction in **4**) the overall redox series is represented as:



Interestingly in **3** we get the above equilibria along with another one which is:

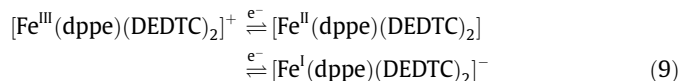


Table 8

Cyclic voltammetric parameters of **1**, **3** and **4**. Potentials are in volts (V) vs. SCE at 25 °C and 760 mm.

Entry	Anodic potential (Epa)	Cathodic potential (Epc)	ΔE_r (mv)	Assignment
1 [Fe(dppe)(DEDTC) ₂]CH ₂ Cl ₂	+0.86	+0.80	60	Fe ^{III} ⇌ Fe ^{IV}
	−0.22	−0.28	60	Fe ^{III} ⇌ Fe ^{II}
3 [Fe ^{III} (dppe)(DEDTC) ₂][Fe ^{III} Cl ₄]	+0.48	+0.42	60	Fe ^{III} ⇌ Fe ^{IV}
[FeCl ₄] [−]	+0.05	+0.04	90	Fe ^{III} ⇌ Fe ^{II} for the anion
	−0.30	−0.40	100	Fe ^{III} ⇌ Fe ^{II} for the cation
4 [Fe(dppe)(DEDTC) ₂][BPh ₄]	+0.87			Epa of Fe ^{III} → Fe ^{IV}
	−0.22	−0.31	90	Fe ^{III} ⇌ Fe ^{II}

This redox picture actually attests the molecular composition of the complexes studied, besides displaying the potentials (in Volts versus SCE) of the redox reactions.

4. Concluding remarks

This work discovers that iron (III) complexes with $\text{Fe}^{\text{III}}\text{S}_4\text{P}_2$ functionality for example, **3** and **4** (see text) possessing two *N,N*-diethyldithiocarbamate (DEDTC; S_4) and one 1,2-bis (diphenylphosphino) ethane (dppe; P_2) ligands, lie on the right side of spin crossover zone of the Tanabe Sugano diagram. So, these types of Fe (III) complexes are all expected to show low-spin behavior in the entire temperature range of 2–300 K. We expect that our (immediate) next work will be able to define the left side boundaries of the said diagram and the Fe (III) complexes lying on the left side of that boundary will exhibit only high spin behavior in the said temperature range. Then we shall get an entire midfield range accessible by the directed synthesis of Fe (III) complexes possessing slightly lower field strength than the right side and also by the complexes having a little higher field strength than the left side. Midfielder molecules can be synthesized by modifying or changing the ligand, so as to possess the right ligand field effect. All those molecules will then show spin–transition behavior and can be used in optoelectronics, information storage and other important properties as mentioned in Section 1.

Acknowledgements

The authors namely T.K.J., D.P.K., S.D. and R.B. thank Department of Science and Technology (DST), Govt. of India for financial assistance in the form of a Project (Project No. SR/S1/IC-12/2002). T.K.J. thanks DST and D.P.K. thank CSIR, Govt. of India, for fellowship. The magnetic and Mössbauer studies have been supported by the Centre Franco-Indien pour la promotion de la Recherche Avancée/Indo-French Centre for the Promotion of Advanced Research under Project No. 3108-3.

Appendix A. Supplementary material

CCDC 639617, 639618 and 639619 contain the supplementary crystallographic data for **1**, **3** and **5**. These data can be obtained free of charge from The Cambridge Crystallographic Data Centre via www.ccdc.cam.ac.uk/data_request/cif. Supplementary data associated with this article can be found, in the online version, at [doi:10.1016/j.ica.2009.04.007](https://doi.org/10.1016/j.ica.2009.04.007).

References

- [1] L. Cambi, L. Szego, *Chem. Ber.* 10 (1931) 2591.
- [2] L. Cambi, L. Szego, *Chem. Ber.* 16 (1933) 656.
- [3] Y. Tanabe, S. Sugano, *J. Phys. Soc. Jpn.* 9 (1954) 753.
- [4] I. Krivokapic, C. Euachescu, R. Browisz, A. Hansen, *Chem. Phys. Lett.* 455 (2006) 192.
- [5] V. Escax, A. Bluezen, C. dit Moulin Cartier, F. Villain, A. Goujou, E. Varret, M. Verdagner, *J. Am. Chem. Soc.* 123 (2001) 12536.
- [6] O. Kahn, J. Kröber, C. Jay, *Adv. Mater.* 4 (1982) 718.
- [7] K. Boukheddaden, J. Shito, B. Hoo, F. Varret, *Phys. Rev. B* 62 (2000) 14796.
- [8] Y. Galimedinov, V. Kaenofantov, A. Provisin, I. Orchinnikov, G. Ivanova, P. Gütlich, W. Haase, *Angew. Chem., Int. Ed.* 113 (2001) 4399.
- [9] W.R. Schiet, C.A. Rome, *Chem. Rev.* 81 (1981) 543.
- [10] R.W. Noble, A. de Young, D.L. Rousseau, *Biochemistry* 28 (1989) 5293.
- [11] C.K. Jorgensen, *Modern Aspects of Ligand Field Theory*, Elsevier, New York, 1997.
- [12] B. Douglas, D. McDaniel, J. Alexander, in: *Concepts and models of Inorganic Chemistry*, 3rd ed., John Wiley and Sons (Asia), Singapore, 2001.
- [13] N. Weberg, *Inorganic Chemistry*, Academic Press, New York, 2001.
- [14] J.E. Huheey, E.A. Keiter, R.L. Keiter in: *Inorganic Chemistry, Principles of Structure and Reactivity*, 4th ed., Harper and Collins College Publishers, New York, 1993, Reprinted in India.
- [15] J.D. Lee, in: *Concise Inorganic Chemistry*, 4th ed., ELBS and Chapman & Hall, Singapore, 1994.
- [16] N.N. Greenwood, A. Earnshaw, in: *Chemistry of the Elements*, 2nd ed., Butterworth Heineman, London, UK, 1997.
- [17] A.B. Gaspar, M.C. Munoz, V. Niel, J.A. Real, *Inorg. Chem.* 40 (2001) 9.
- [18] H.A. Goodwin, *Top. Curr. Chem.* 234 (2004) 23.
- [19] J.E. Huheey, *Inorganic Chemistry: Principles of Structure and Reactivity*, Harper and Raw, London, UK, 1975.
- [20] A.H. Ewald, R.L. Martin, I.G. Ross, A.H. White, *Proc. R. Soc. Lond., Ser. A* 280 (1964) 235.
- [21] A.H. White, E. Kokot, R. Roper, H. Waterman, R.L. Martin, *Aust. J. Chem.* 17 (1964) 294.
- [22] A.H. Ewald, R.L. Martin, E. Sinn, A.H. White, *Inorg. Chem.* 8 (1969) 1837.
- [23] T. Glaser, B. Hedman, K.O. Hodgson, E.I. Solomon, *Acc. Chem. Res.* 33 (2000) 859.
- [24] F.A. Cotton, G. Wilkinson, *Advanced Inorganic Chemistry*, 3rd ed., Wiley Eastern Ltd., New Delhi, 1978.
- [25] Tetraphenyl phosphonium salt of FeCl_4^- has not yet been reported, though the complex associated with other organic counter cations are known. C. Furlani, E. Cervone, V. Valenti, *J. Inorg. Nucl. Chem.* 25 (1963) 159.
- [26] R. Pradhan, S.P. Mukhopadhyay, D.C. Bera, C. Simonnet, F. Secheresse, R. Bhattacharyya, *Inorg. Chem. Commun.* 2 (1999) 495.
- [27] F.A. Cotton, G. Wilkinson, C.A. Murillo, M. Bochmann, in: *Advanced Inorganic Chemistry*, 6th ed., John Wiley and Sons, New York, 1999, p. 793.
- [28] G.H. Spikes, E.Bill.T. Weyhermueller, K. Wieghardt, *Chem. Commun.* (2007) 4339, and references cited therein.
- [29] K. Mayer, E. Bill, E. Minert, T. Weyhermueller, K. Wieghardt, *J. Am. Chem. Soc.* 121 (1999) 4859.
- [30] A.I. Vogel, in: *A Text Book of Practical Organic Chemistry including Qualitative Organic Analysis*, 3rd ed., Longman, London, 1968, p. 499.
- [31] J. Hesse, A. Rubartsch, *J. Phys. E Sci. Instrum.* 7 (1974) 526.
- [32] A. Müller, R. Jostes, W. Eltzner, C.S. Nie, E. Diemann, H. Bögge, M. Zimmermann, M. Dartmann, U. Reinsch-Vogel, S. Che, S.J. Cyvin, B.N. Cyvin, *Inorg. Chem.* 14 (1985) 2872.
- [33] R. Bhattacharyya, P.K. Chakrabarty, P.N. Ghosh, A.K. Mukherjee, D. Podder, M. Mukherjee, *Inorg. Chem.* 30 (1991) 3948.
- [34] APEX2 Version 1.0-8; Bruker AXS: Madison, WI, 2003.
- [35] SHELXL Version 6.14; Bruker AXS: Madison, WI, 2001.
- [36] G.M. Sheldrick, SADABS, A Program for the Siemens Area Detector Absorption Correction, 1994.
- [37] R.H. Blessing, *Acta Crystallogr.* A51 (1995) 33.
- [38] G.M. Sheldrick, SHELXL, Siemens Analytical X-ray Instruments, 1994.
- [39] G.M. Sheldrick, in: *Program for the Refinement of Crystal Structures*, 1997.
- [40] W.J. Geary, *Coord. Chem. Rev.* 7 (1971) 81.
- [41] D.C. Bradley, M.H. Gitlitz, *J. Chem. Soc. A* (1969) 1152.
- [42] C. O'Connor, J.D. Gilbert, G. Wilkinson, *J. Chem. Soc. A* (1969) 84.
- [43] L.H. Little, G.W. Poling, J. Leja, *Can. J. Chem.* 39 (1961) 745.
- [44] C.W. Watt, B.J. McCormick, *Spectrochim. Acta* 21 (1965) 753.
- [45] C. Udovich, J. Takemoto, K. Nakamoto, *J. Coord. Chem.* 1 (1971) 89.
- [46] B. Hutchinson, P. Neill, A. Finkelstein, J. Takemoto, *Inorg. Chem.* 20 (1981) 2000.
- [47] J.S. Evary, C.D. Burbridge, D.M.L. Goodgame, *Spectrochim. Acta* 24A (1968) 1721.
- [48] K. Nakamoto, in: *Infrared and Raman Spectra of Inorganic and coordination Compounds*, 4th ed., John Wiley, New York, 1986, p. 133.
- [49] B.N. Figgis, in: *Introduction to Ligand Fields*, John Wiley Interscience, New York, 1966, p. 163.
- [50] S. Ahrland, J. Chatt, N.R. Davies, *Quart. Rev.* 12 (1958) 265.
- [51] G. Klopman, *J. Am. Chem. Soc.* 90 (1968) 223.
- [52] M. Biner, H.B. Bürje, A. Ludi, C. Röhr, *J. Am. Chem. Soc.* 114 (1992) 5197.
- [53] R. Shaviv, C.B. Lowe, J.A. Zora, C.B. Aakeröy, P.B. Hitchcock, K.R. Seddon, R.L. Carlin, *Inorg. Chim. Acta* 198–200 (1992) 613.
- [54] A. Chakrobarty, K. Nag, *Coord. Chem. Rev.* 33 (1980) 87.
- [55] H.H. Wickman, A.M. Trozzolo, H.J. William, G.W. Hull, F.R. Merritt, *Phys. Rev.* 155 (1967) 563.
- [56] T. Sato, F. Ambe, T. Kitazawa, H. Sano, M. Takeda, *Chem. Lett.* (1997) 1287.
- [57] A.P. Ginsberg, M.B. Robin, *Inorg. Chem.* 2 (1963) 817.
- [58] G.L. Miesler, D.A. Tarr, in: *Inorganic Chemistry*, 2nd ed., Prentice Hall International, New Jersey, 1991.